



High-pressure and high-temperature synthesis of heavy lanthanide sesquisulfides Ln_2S_3 ($Ln=Yb$ and Lu)



Masatoshi Kanazawa ^a, Liang Li ^a, Toshihiro Kuzuya ^a, Keiki Takeda ^a, Shinji Hirai ^a, Yuji Higo ^b, Toru Shinmei ^c, Tetsuo Irifune ^c, Chihiro Sekine ^{a,*}

^a Muroran Institute of Technology, Muroran, 050-8585, Japan

^b Japan Synchrotron Radiation Institute, Hyogo, 679-5198, Japan

^c Geodynamics Research Center, Ehime University, Ehime, 790-8577, Japan

ARTICLE INFO

Article history:

Received 31 August 2017

Received in revised form

6 November 2017

Accepted 7 November 2017

Available online 10 November 2017

Keywords:

High-pressure synthesis

Sesquisulfide

In-situ x-ray diffraction

Crystal structure

ABSTRACT

Detailed pressure-temperature phase diagrams of heavy lanthanide sesquisulfides Ln_2S_3 ($Ln = Yb$ and Lu) have been investigated by in-situ x-ray diffraction experiments under high pressure and high temperature using synchrotron radiation and multi-anvil press. Based on the results of the in-situ observation, the single γ -phase (Th_3P_4 -type structure, $I\bar{4}3d$) samples of Ln_2S_3 ($Ln = Yb$ and Lu) have been synthesized under high pressure. The physical properties of the compounds were studied by electrical resistivity, specific heat, and magnetic susceptibility measurements between 2 K and 300 K.

© 2017 Elsevier B.V. All rights reserved.

1. Introduction

Heavy-lanthanide sesquisulfides Ln_2S_3 ($Ln =$ Lanthanide) have seven forms of crystal structure [1]. Among them, the γ -phase (cubic, $I\bar{4}3d$), which has Th_3P_4 -type structure, is expected for high-performance thermoelectric materials or optical materials [2–4]. However, the γ -phase of heavy-lanthanide sesquisulfides Ln_2S_3 are difficult to synthesize at ambient pressure. While it has been reported that Lu_2S_3 was about 50% converted from the ϵ phase (rhombohedral, $R\bar{3}c$) to the γ -phase under high pressure and high temperature [5], a high-quality single phase sample of γ - Lu_2S_3 has not been obtained so far. In this study, we have tried to synthesize samples of γ - Lu_2S_3 under high pressure using a low-pressure phase (named ζ -phase, orthorhombic Sc_2S_3 -type structure, $Fddd$) [6] and the elements as starting materials. In order to obtain the optimum condition for preparing high-quality samples of γ - Lu_2S_3 under high pressure, detailed pressure-temperature (P-T) phase diagrams of Lu_2S_3 and a analogue compound Yb_2S_3 for comparison have been investigated by in-situ x-ray diffraction experiments using synchrotron radiation. Based on the optimum condition decided by the

in-situ observation, the single γ -phase samples of Ln_2S_3 ($Ln = Yb$ and Lu) have been synthesized. Furthermore, the fundamental physical properties have been investigated.

2. Experimental

In-situ x-ray diffraction patterns were taken by an energy dispersive method using synchrotron radiation and a solid-state detector. High pressure was applied using a multi-anvil assembly 6-6 (MA6-6) [7] with a cubic-anvil high-pressure apparatus, the MAX80 system, installed at the beam line AR-NE5C, at Photon Factory (PF) in High Energy Accelerator Research Organization (KEK) (Tsukuba, Japan). The MA6-6 consists of six small second-stage anvils with an anvil guide, and can be compressed by a cubic-anvil apparatus. The truncated edge length (TEL) of the second-stage anvil made of tungsten carbide is 4 mm. The anvil guide is made of tool steel (SUS304), with an outer edge length of 28 mm. The anvil guide has holes along one of the diagonal direction for access to the incident and exiting x-rays. The TEL of the first-stage anvil is 27 mm. The sample container made of phryophilite is formed into a cube of 7 mm on an edge. The starting materials, which are ζ -phase ($Fddd$) powder samples or mixture of rare earth metals and sulfur, are put into a BN crucible. The crucible with a graphite heater is inserted in a cube-shaped phryophilite

* Corresponding author.

E-mail address: sekine@mmm.muroran-it.ac.jp (C. Sekine).

solid pressure medium. Pressure was determined by the lattice constant of NaCl internal pressure marker. The details of the in-situ observation method were described in previous report [8]. To measure in-situ x-ray diffraction pattern of Lu_2S_3 above 8 GPa, we used a Kawai-type double-stage multi-anvil high-pressure apparatus, the SPEED-1500 system [9], installed at the beam line BL04B1 at SPring-8, Japan. The powder samples of $\zeta\text{-Yb}_2\text{S}_3$ and $\zeta\text{-Lu}_2\text{S}_3$ for the starting materials were synthesized by means of CS_2 gas sulfidation method [10].

X-ray powder diffraction patterns of $\zeta\text{-Lu}_2\text{S}_3$ ($Fddd$) at room temperature and high pressures were measured with a diamond-anvil cell (DAC) and an imaging plate using synchrotron radiation. High-pressure diffraction experiments were performed at the beam line 18C at PF in KEK. We employed the DAC with diamond culet diameters of 500 μm . The sample was finely ground and loaded in the 180 μm diameter hole drilled in a stainless steel (T301) gasket. The pressure in the DAC was measured before and after each exposure based on the shifts of the ruby R1 and R2 fluorescence lines. A 4:1 methanol-ethanol solution was used as the pressure medium.

Large bulk samples of $\gamma\text{-Yb}_2\text{S}_3$ and $\gamma\text{-Lu}_2\text{S}_3$ ($I\bar{4}3d$) were prepared at high temperatures and high pressures using a Kawai-type multi-anvil high-pressure apparatus. The sample cell assembly is similar to that used for the high-pressure synthesis of filled skutterudite compounds [11,12]. The compounds were prepared by transition from ζ -phases ($Fddd$) or reacting stoichiometric amounts of 3N (99.9% pure)-Yb, Lu chips, and 6N-S powder at 3–8 GPa. The reaction temperatures were between 1200 and 1800 $^\circ\text{C}$. The prepared samples were characterized by powder x-ray diffraction using Co

$\text{K}\alpha_1$ radiation and silicon as a standard. The chemical compositions were verified by scanning electron microscope (SEM) with energy dispersive x-ray spectrometer (EDX, JEOL). Resistivity was measured by a standard dc four-probe method. Magnetization was measured with a Quantum Design MPMS superconducting quantum interference device magnetometer. The specific heat was measured by a thermal relaxation method (PPMS; Quantum Design).

3. Results and discussion

3.1. Sample preparation and P-T phase diagram of Yb_2S_3

Fig. 1 shows some of the in-situ x-ray diffraction patterns of Yb_2S_3 using $\zeta\text{-Yb}_2\text{S}_3$ ($Fddd$) powder as starting materials. Fig. 1(a) shows x-ray diffraction pattern of the starting material $\zeta\text{-Yb}_2\text{S}_3$ ($Fddd$) at room temperature and 3 GPa. Solid squares indicate the characteristic x-ray for Yb. Open circles indicate the Bragg peaks of $\zeta\text{-Yb}_2\text{S}_3$ ($Fddd$). On increasing the pressure, no changes in the diffraction patterns could be observed except shifting of peaks due to lattice compression. This trend is observed until 5.5 GPa. Absence of any additional diffraction peak with pressure indicates that the material is structurally stable under compression up to 5.5 GPa at least. With increasing temperature, the Bragg peaks of $\zeta\text{-Yb}_2\text{S}_3$ ($Fddd$) faded out, and then the peaks of $\text{YbS}_{1.7}$ (tetragonal NdS_2 -type structure [13], $P\bar{4}b2$) were observed above 400 $^\circ\text{C}$ (Fig. 1(b)). At the same time, Yb oxysulfide $\text{Yb}_2\text{O}_2\text{S}$ (monoclinic, $P2_1/c$) [14] as an impurity phase was detected. Above 1100 $^\circ\text{C}$ $\text{YbS}_{1.7}$ ($P\bar{4}b2$) started to change to III- Yb_2S_3 (orthorhombic U_2S_3 -type structure [1], $Pnma$)

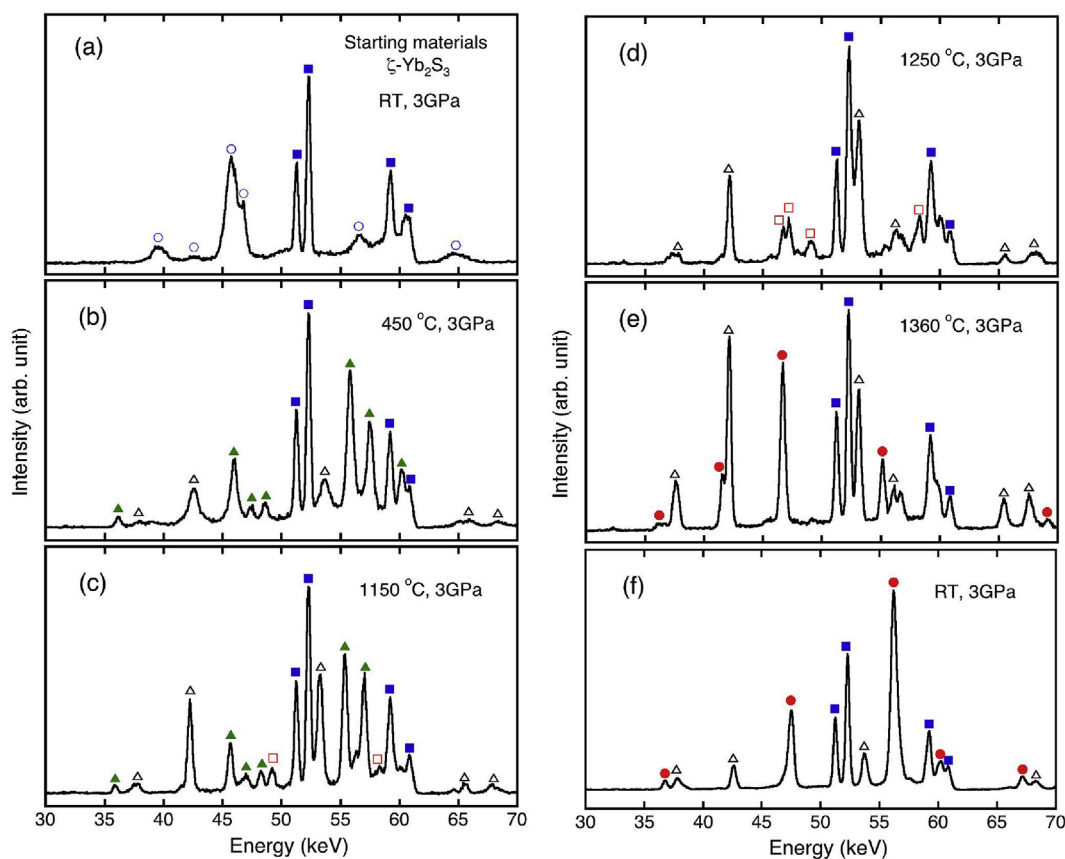


Fig. 1. X-ray diffraction patterns of heating process of $\zeta\text{-Yb}_2\text{S}_3$ ($Fddd$) at 3 GPa. Open circles designate the Bragg peaks of $\zeta\text{-Yb}_2\text{S}_3$ ($Fddd$). Solid squares indicate the characteristic x-ray for Yb. Solid triangles, open squares and solid circles designate the Bragg peaks of $\text{YbS}_{1.7}$ ($P\bar{4}b2$), III- Yb_2S_3 ($Pnma$) and $\gamma\text{-Yb}_2\text{S}_3$ ($I\bar{4}3d$), respectively. Open triangles indicate the peaks of $\text{Yb}_2\text{O}_2\text{S}$ ($P2_1/c$). (a) The starting materials ($\zeta\text{-Yb}_2\text{S}_3$) at room temperature, (b) 450 $^\circ\text{C}$, (c) 1150 $^\circ\text{C}$, (d) 1250 $^\circ\text{C}$, (e) 1360 $^\circ\text{C}$ and (f) room temperature after quenching.

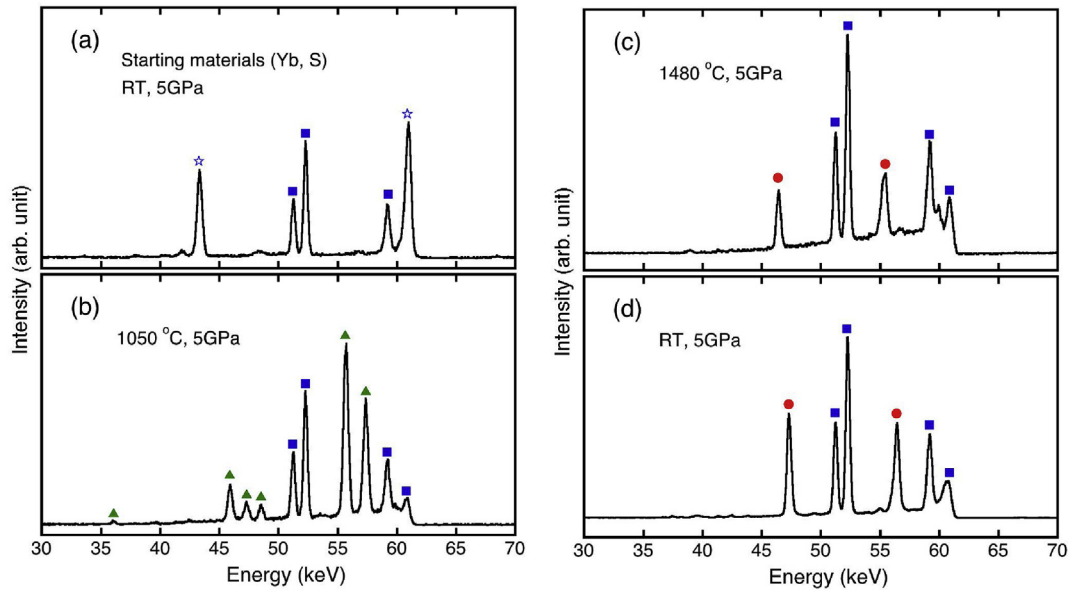


Fig. 2. X-ray diffraction patterns of synthesizing process of Yb_2S_3 at 5 GPa. Open stars indicate the Bragg peaks of Yb and solid squares indicate the characteristic x-ray for Yb. Solid triangles and solid circles designate the Bragg peaks of $\text{YbS}_{1.7}$ ($P\bar{4}b2$) and $\gamma\text{-Yb}_2\text{S}_3$ ($I\bar{4}3d$), respectively. (a) The starting materials at room temperature, (b) 1050 °C, (c) 1480 °C and (d) room temperature after quenching.

(Fig. 1(c)) and at 1250 °C the Bragg peaks of $\zeta\text{-Yb}_2\text{S}_3$ ($Fddd$) disappeared and the peaks of $\text{III-Yb}_2\text{S}_3$ ($Pnma$) and $\text{Yb}_2\text{O}_2\text{S}$ ($P2_1/c$) were observed (Fig. 1(d)). With increasing temperature up to 1360 °C, $\text{III-Yb}_2\text{S}_3$ ($Pnma$) made phase transition to $\gamma\text{-Yb}_2\text{S}_3$ ($I\bar{4}3d$) (Fig. 1(e)). After a temperature quench, γ -phase ($I\bar{4}3d$) was also observed (Fig. 1(f)). In series of the experiments at several pressures, we summarized P-T phase diagram of Yb_2S_3 using $\zeta\text{-Yb}_2\text{S}_3$ ($Fddd$) as starting materials in Fig. 3(a).

Fig. 2 shows the x-ray diffraction patterns of synthesizing process of Yb_2S_3 using the starting materials, which are mixture of Yb and S powder in the atomic ratio of Yb: S = 2: 3, at 5 GPa. Fig. 2(a) shows x-ray diffraction pattern of the starting material at room temperature. Open stars designate the Bragg peaks of Yb and solid squares indicate the characteristic x-ray for Yb. With increasing temperature, the Bragg peaks of Yb faded out, and then the peaks of $\text{YbS}_{1.7}$ ($P\bar{4}b2$) were observed above 400 °C (Fig. 2(b)). With increasing temperature up to 1480 °C, $\text{YbS}_{1.7}$ ($P\bar{4}b2$) made phase transition to $\gamma\text{-Yb}_2\text{S}_3$ ($I\bar{4}3d$) (Fig. 2(c)). After a temperature quench, γ -phase ($I\bar{4}3d$) was also observed (Fig. 2(d)). In series of the experiments at several pressures, we summarized P-T phase diagram of Yb_2S_3 using Yb and S elements as starting materials in Fig. 3(b).

In this study, using the ζ -phase ($Fddd$) as the starting material, P-T phase diagram of Yb_2S_3 was obtained for the first time while P-T phase diagram of Yb_2S_3 using the ε -phase ($R\bar{3}c$) as the starting material has been reported [1]. As shown in Fig. 3(a), II-phase (monoclinic F-type structure, $P2_1/m$) [1] and III-phase ($Pnma$) were observed. The results are consistent with previous report [1]. Furthermore, $\zeta\text{-Yb}_2\text{S}_3$ ($Fddd$) shows the transition to $\text{YbS}_{1.7}$ ($P\bar{4}b2$) and subsequently to γ -phase ($I\bar{4}3d$). The transition from $\text{YbS}_{1.7}$ ($P\bar{4}b2$) to γ -phase ($I\bar{4}3d$) via III-phase ($Pnma$) was also observed around 3 GPa. On the other hand, II-phase ($P2_1/m$) and III-phase ($Pnma$) were not observed in P-T phase diagram of Yb_2S_3 using Yb and S elements as starting materials (Fig. 3(b)), which is consistent with previous report [13]. As shown in Fig. 3(b), Yb reacts with S to form $\text{YbS}_{1.7}$ ($P\bar{4}b2$) at first and then changes to γ -phase ($I\bar{4}3d$) same as previous report [13]. We expand the region of the P-T phase diagram using elements as starting materials up to 5 GPa and 1500 °C.

We have actually synthesized $\gamma\text{-Yb}_2\text{S}_3$ ($I\bar{4}3d$) at 3 GPa and

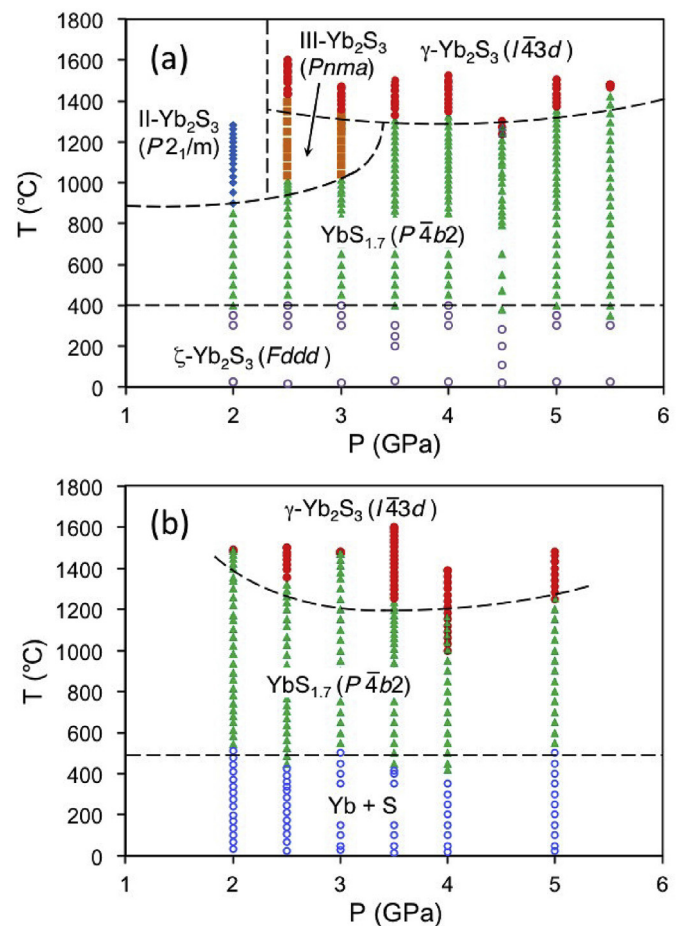


Fig. 3. (a) P-T phase diagram of Yb_2S_3 using $\zeta\text{-Yb}_2\text{S}_3$ ($Fddd$) as starting materials. Open circles, solid triangles, solid diamonds, solid squares and solid circles designate ζ -phase ($Fddd$), $\text{YbS}_{1.7}$ -phase ($P\bar{4}b2$), II-phase ($P2_1/m$), III-phase ($Pnma$) and γ -phase ($I\bar{4}3d$) observed by the in-situ x-ray diffraction experiments, respectively. (b) P-T phase diagram of Yb_2S_3 using Yb and S elements as starting materials. Open circles, solid triangles and solid circles designate starting materials (Yb, S), $\text{YbS}_{1.7}$ -phase ($P\bar{4}b2$) and γ -phase ($I\bar{4}3d$) observed by the in-situ x-ray diffraction experiments, respectively.

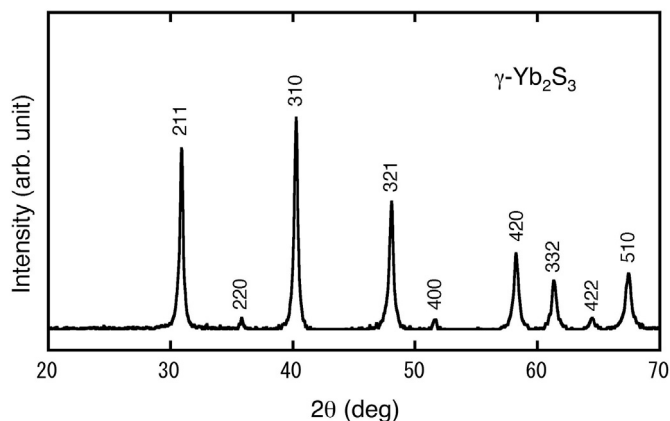


Fig. 4. X-ray diffraction patterns of γ - Yb_2S_3 ($I\bar{4}3d$) prepared under 3 GPa.

1400 °C using a Kawai-type multi-anvil high-pressure apparatus based on the synthesis condition obtained by the in-situ experiments. Fig. 4 shows x-ray diffraction patterns of γ - Yb_2S_3 ($I\bar{4}3d$) prepared under high pressure using mixture of Yb and S powder in the atomic ratio of Yb: S = 2: 3 as the starting materials. The most observed diffraction lines were indexable using the Th_3P_4 -type structure. Using elements as the starting materials, single phase sample of γ - Yb_2S_3 ($I\bar{4}3d$) was obtained. The lattice parameter determined by a least-squares fit of indexed peaks to d-spacing formula is given in Table 1 along with the literature value [5]. To determine the actual element distribution, elemental mapping and point analysis of SEM-EDX were conducted. For the point analysis, dozens of different points were carefully chosen to reduce errors. The point analysis implies that a fluctuation of the composition around 2%. The analyzed composition decided by SEM-EDX is also given in Table 1.

3.2. X-ray powder diffraction of ζ - Lu_2S_3 under high pressure at room temperature

It has been reported that a reversible phase transition from ε - Lu_2S_3 ($R\bar{3}c$) to γ -phase ($I\bar{4}3d$) above 5 GPa at room temperature [15]. Therefore, in order to investigate the stability of ζ - Lu_2S_3 ($Fddd$) under high pressure, we have studied the x-ray powder diffraction of ζ - Lu_2S_3 with the DAC up to 12.4 GPa at room temperature. Lattice parameters at each pressure are given in Table 2. Fig. 5 shows powder x-ray diffraction patterns of ζ - Lu_2S_3 (wavelength $\lambda = 0.6199$ Å) at room temperature and high pressures. Absence of any additional diffraction peak with pressure indicates that the compound is structurally stable under compression up to 12.4 GPa. Fig. 6 shows the relative cell volume (V/V_0) vs. pressure curve for ζ - Lu_2S_3 . The cell volume of ζ - Lu_2S_3 monotonically decreases with increasing pressure up to 12.4 GPa. The data can be fitted by the

Table 1

Crystal data and lattice parameters decided by x-ray diffraction and analyzed compositions decided by SEM-EDX of the γ -lanthanide sulfides prepared under high pressure.

Compound	Yb_2S_3	Lu_2S_3
Crystal system	Cubic	Cubic
Space group	$I\bar{4}3d$	$I\bar{4}3d$
Lattice parameter a(Å)		
This work	8.214(1)	8.182(2)
Reference [5]	8.224	8.198
Analyzed mole ratio S/Ln decided by SEM-EDX	1.41–1.44	1.39–1.44

Table 2

Lattice parameters a, b, c and cell volume V of ζ - Lu_2S_3 (orthorhombic, $Fddd$) decided by x-ray diffraction at each pressure and room temperature.

Pressure (GPa)	a(Å)	b(Å)	c(Å)	V(Å ³)
0.3	10.7976(2)	7.7076(2)	22.9543(5)	1910.34(7)
3.2	10.6357(2)	7.5732(2)	22.6635(6)	1825.47(7)
6.0	10.5019(3)	7.4526(2)	22.4077(8)	1753.78(9)
8.5	10.4013(3)	7.3557(3)	22.2008(7)	1698.5(1)
12.4	10.299(1)	7.2427(6)	21.971(2)	1638.9(2)

Birch equation of state [16]:

$$P = \frac{3}{2}B_0 \left\{ \left(\frac{V}{V_0} \right)^{-\frac{7}{3}} - \left(\frac{V}{V_0} \right)^{-\frac{5}{3}} \right\} \left[1 - \frac{3}{4}(4 - B_0') \left\{ \left(\frac{V}{V_0} \right)^{-\frac{2}{3}} - 1 \right\} \right] \quad (1)$$

where B_0 , B_0' , V and P are the bulk modulus, its first derivative, the volume and pressure. A least-squares fit to the data of ζ - Lu_2S_3 gives the following values: $B_0 = 56(3)$ GPa and $B_0' = 4.2(8)$.

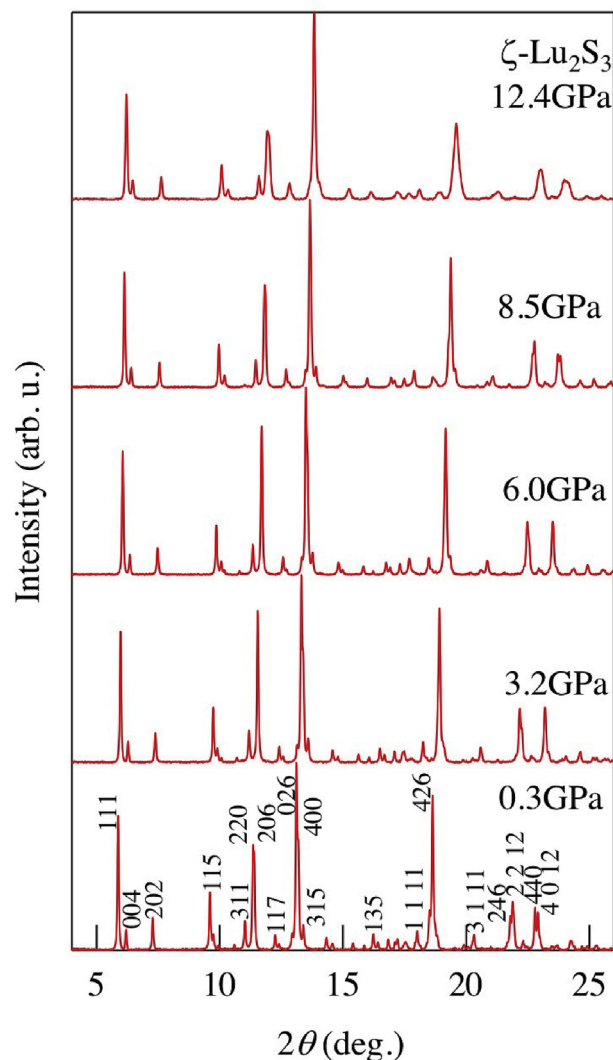


Fig. 5. X-ray diffraction patterns of ζ - Lu_2S_3 ($Fddd$) at room temperature and high pressures.

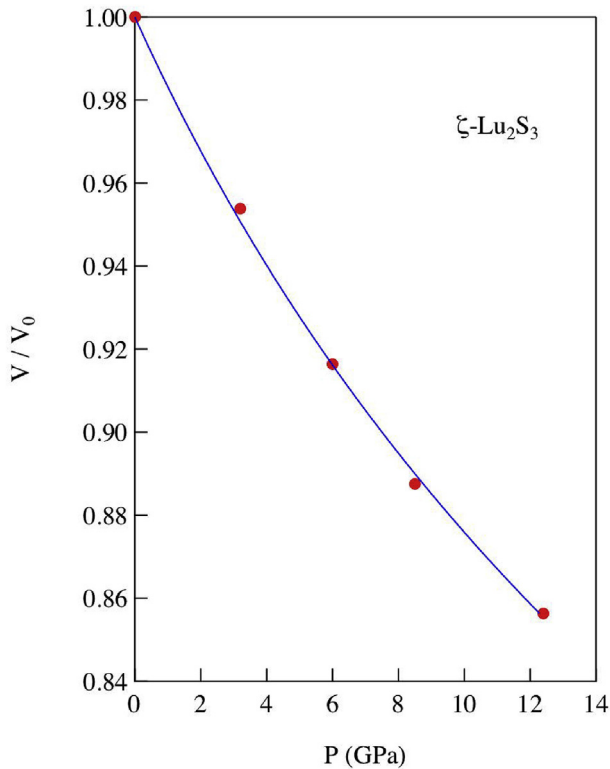


Fig. 6. Relative cell volume plotted as a function of pressure for ζ - Lu_2S_3 ($Fddd$).

3.3. Sample preparation and P-T phase diagram of Lu_2S_3

Fig. 7 shows some of the in-situ x-ray diffraction patterns of Lu_2S_3 using ζ - Lu_2S_3 ($Fddd$) powder as starting materials. Fig. 7(a) shows x-ray diffraction pattern of the starting material ζ - Lu_2S_3 ($Fddd$) at room temperature and 10 GPa (Solid squares). The characteristic x-ray of Lu and Bragg peaks of ζ - Lu_2S_3 ($Fddd$) were

observed. Absence of any additional diffraction peak with pressure indicates that the phase is stable up to 10 GPa already shown above. With increasing temperature up to 500 °C, ζ - Lu_2S_3 ($Fddd$) made phase transition to $\text{LuS}_{1.7}$ (tetragonal, $P4nmm$) (Fig. 7(b)). At the same time, Lu oxysulfide $\text{Lu}_2\text{O}_2\text{S}$ ($P2_1/c$) as an impurity phase was detected same as Yb_2S_3 . Above 800 °C $\text{LuS}_{1.7}$ ($P4nmm$) made phase transition to $\text{LuS}_{1.7}$ ($P4b2$) (Fig. 7(c)). In the temperature range up to 1500 °C, a transition from $\text{LuS}_{1.7}$ ($P4b2$) to γ -phase ($I43d$) was not observed at 10 GPa (Fig. 7(d)). After a temperature quench, $\text{LuS}_{1.7}$ ($P4b2$) was also observed (Fig. 7(e)). In series of the experiments at several pressures, we summarized P-T phase diagram of Lu_2S_3 using ζ -phase ($Fddd$) as starting materials in Fig. 8(b). Using the ζ -phase ($Fddd$) as the starting material, P-T phase diagram of Lu_2S_3 was obtained for the first time while P-T phase diagram of Lu_2S_3 using the ϵ -phase ($R\bar{3}c$) as the starting material has been reported [1]. As shown in Fig. 8(b), transitions to II ($P2_1/m$) and III ($Pnma$) phases via $\text{LuS}_{1.7}$ ($P4b2$) were observed. The results are consistent with previous report [1]. However, IV-phase (orthorhombic, NdYbS_3 -type, $C222_1$) and γ -phase ($I43d$) were not detected in the observed range (up to 10 GPa and 1500 °C).

It has been reported that Lu_2S_3 was about 50% converted from the ϵ phase ($R\bar{3}c$) to the γ -phase ($I43d$) under 7.7 GPa and 2000 °C [5]. Therefore, we have investigated P-T phase diagram of Lu_2S_3 in the range up to 7 GPa and 1800 °C by quenching experiments using elements as the starting materials. In series of the experiments at several pressures, we summarized P-T phase diagram of Lu_2S_3 using elements as starting materials in Fig. 8(a). γ -phase ($I43d$) was detected at 1800 °C from 5 GPa to 7 GPa.

Fig. 9 shows x-ray diffraction pattern of γ - Lu_2S_3 ($I43d$) prepared at 7 GPa and 1800 °C using mixture of Lu and S powder in the atomic ratio of Yb: S = 2: 3 as the starting materials. The most observed diffraction lines were indexable using the Th_3P_4 -type structure while a small amount of impurity phase (Lu oxysulfide, open triangles). The lattice parameter determined by a least-squares fit of indexed peaks to d-spacing formula is given in Table 1 along with the literature values [5]. To determine the actual element distribution, elemental mapping and point analysis of SEM-EDX were conducted. The point analysis implies that a

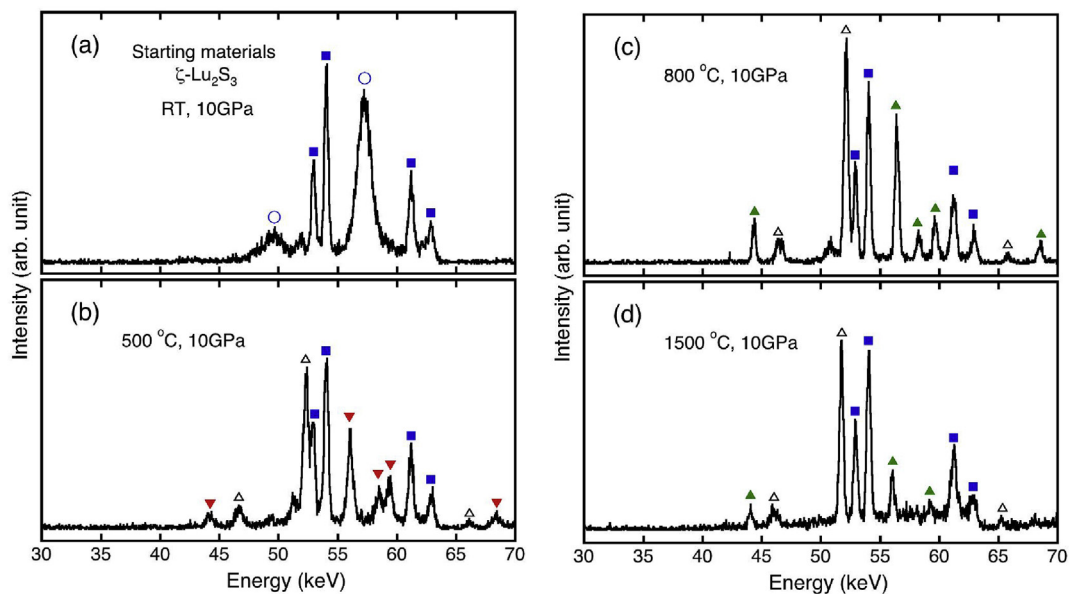


Fig. 7. X-ray diffraction patterns of heating process of ζ - Lu_2S_3 ($Fddd$) at 10 GPa. Open circles designate the Bragg peaks of ζ - Lu_2S_3 ($Fddd$). Solid squares indicate the characteristic x-ray for Lu. Solid down-pointing triangles and solid triangles designate the Bragg peaks of $\text{LuS}_{1.7}$ ($P4nmm$) and $\text{LuS}_{1.7}$ ($P4b2$), respectively. Open triangles indicate the peaks of $\text{Lu}_2\text{O}_2\text{S}$ ($P2_1/c$). (a) The starting materials at room temperature, (b) 500 °C, (c) 800 °C and (d) 1500 °C.

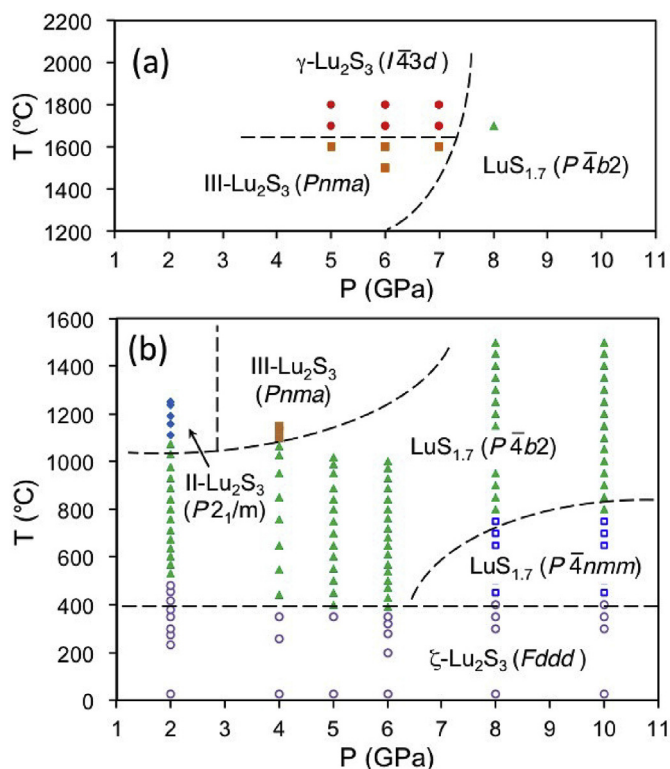


Fig. 8. (a) P-T phase diagram of Lu_2S_3 decided by the quenching experiments using Lu and S elements as starting materials. Solid triangles, solid squares and solid circles designate $\text{YbS}_{1.7}$ -phase ($P\bar{4}b2$), III-phase ($Pnma$) and γ -phase ($I\bar{4}3d$), respectively. (b) P-T phase diagram of Lu_2S_3 using ζ - Lu_2S_3 ($Fddd$) as starting materials. Open circles, solid triangles, solid diamonds, solid squares and open squares designate ζ -phase ($Fddd$), $\text{LuS}_{1.7}$ -phase ($P\bar{4}b2$), II-phase ($P2_1/m$), III-phase ($Pnma$) and $\text{LuS}_{1.7}$ -phase ($P\bar{4}nm$) observed by the in-situ x-ray diffraction experiments, respectively.

fluctuation of the composition around 4%. The analyzed composition decided by SEM-EDX is also given in Table 1.

3.4. Electrical resistivity

Fig. 10 shows the temperature dependence of the electrical resistivity ρ for γ - Yb_2S_3 and γ - Lu_2S_3 . Both compounds show the behavior of semiconductor. However, there is a large discrepancy between the absolute values. As sulfur content decreases, the

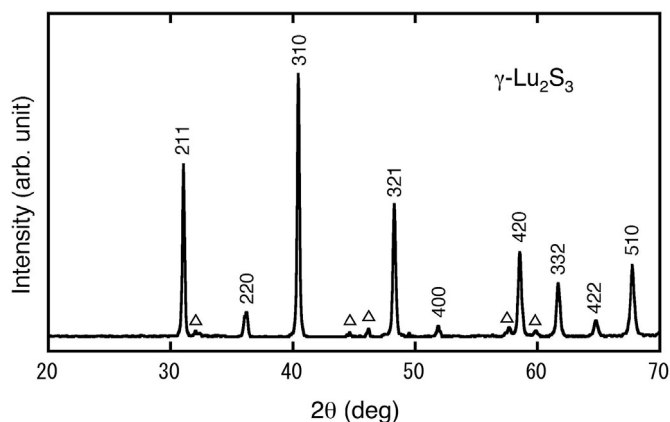


Fig. 9. (a) X-ray diffraction patterns of γ - Lu_2S_3 prepared under 7 GPa. Open triangles indicate the peaks of $\text{Lu}_2\text{O}_2\text{S}$.

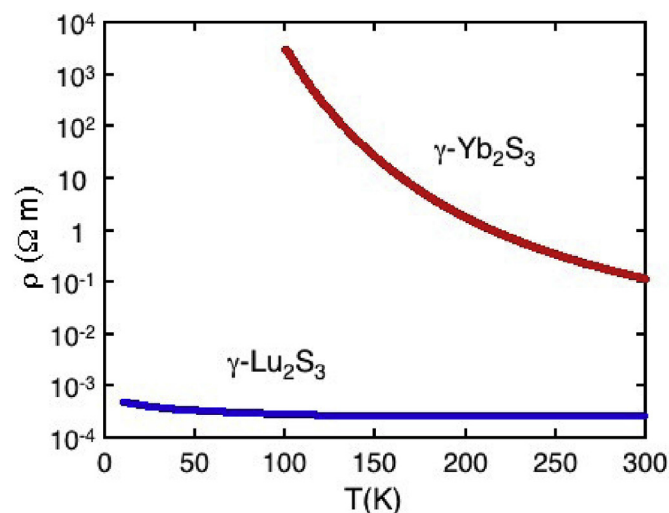


Fig. 10. Temperature dependence of the electrical resistivity for γ - Yb_2S_3 and γ - Lu_2S_3 .

electrical resistivity of rare-earth sesquisulfides tends to decrease because the carrier concentration increases [3]. The atomic ratios of sulfur to rare-earth metal x were 1.41–1.43 for γ - Yb_2S_3 and 1.39–1.44 for γ - Lu_2S_3 by SEM-EDX results (Table 1). The reason for this discrepancy seems to be due to the difference of impurity phases or intrinsic energy gap because there is no essential difference of mole ratios. In order to clarify this point, band calculations and the investigation of sample dependence are desirable.

3.5. Magnetic measurements

Fig. 11 shows the temperature dependences of magnetic susceptibility χ and inverse magnetic susceptibility χ^{-1} at a magnetic field of 1 T for γ - Yb_2S_3 . Above 100 K, $\chi(T)$ can be described by the modified Curie-Weiss law $\chi(T) = \chi_0 + C/(T - \theta_p)$, where C is the Curie constant, θ_p is the paramagnetic Curie temperature and χ_0 is a temperature-independent susceptibility contribution. Least-squares fits from 100 K to 300 K yield effective moments of 4.51–4.53 μ_B/Yb and θ_p is approximately -18 K. The estimated

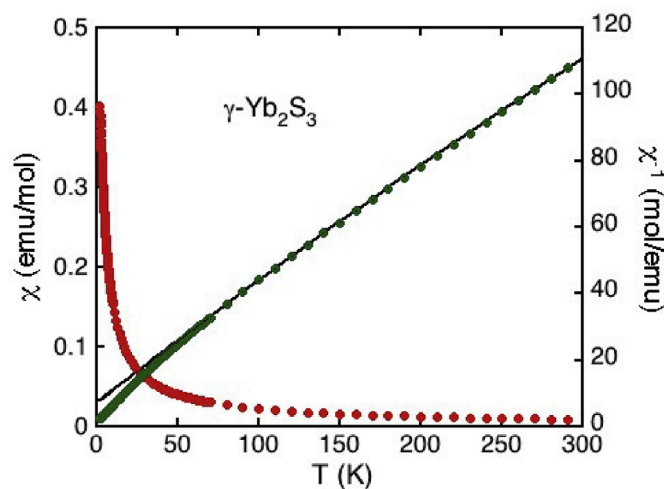


Fig. 11. Temperature dependence of the magnetic susceptibility χ and inverse susceptibility χ^{-1} for γ - Yb_2S_3 at 1 T. The solid line shows a fit to the modified Curie-Weiss law above 100 K.

effective moment is close to the expected value for trivalent Yb of $4.54 \mu_B/\text{Yb}$. This suggests that the Yb ion is trivalent in the compound and the negative θ_p implies an antiferromagnetic correlation. In Fig. 11, the solid line shows a fit to the modified Curie-Weiss law above 100 K.

3.6. Specific heat

Fig. 12 shows temperature dependence of specific heat $C(T)$ for $\gamma\text{-Yb}_2\text{S}_3$ and $\gamma\text{-Lu}_2\text{S}_3$. The $C(T)/T$ data of $\gamma\text{-Lu}_2\text{S}_3$ below 5 K were fitted by $C(T)/T = \gamma + \beta T^2$ (Debye T^3 law); Debye temperature $\theta_D = (12\pi^4 n R / 5 \beta)^{1/3}$, where R is the gas constant and $n = 5$ and γ is the electronic specific heat coefficient. Thus, we obtained $\theta_D = 242$ K and γ is almost zero for $\gamma\text{-Lu}_2\text{S}_3$. Gadzhiev et al. reported Debye temperatures θ_D of $\gamma\text{-Ln}_2\text{S}_3$ ($\text{Ln} = \text{La, Pr, Gd and Dy}$) are 266, 264, 261 and 257 K, respectively [17]. In general, materials with larger masses exhibit smaller Debye temperatures. Thus, $\theta_D = 242$ K for $\gamma\text{-Lu}_2\text{S}_3$ follows this tendency. The inset of Fig. 12 shows enlarged low-temperature region of $C(T)$. An upturn of $C(T)$ for $\gamma\text{-Yb}_2\text{S}_3$ below 8 K was observed. This suggests an appearance of a long-range ordering below around 2 K. This ordering seems to be an antiferromagnetic one because the paramagnetic Curie temperature is negative.

The difference between $\gamma\text{-Yb}_2\text{S}_3$ and $\gamma\text{-Lu}_2\text{S}_3$ could be due to the magnetic contribution of Yb moment. We calculated the magnetic contribution C_{mag} to specific heat of $\gamma\text{-Yb}_2\text{S}_3$ by subtracting the specific heat of $\gamma\text{-Lu}_2\text{S}_3$. Fig. 13(a) shows temperature dependence of C_{mag} for $\gamma\text{-Yb}_2\text{S}_3$. A broad peak is observed around 150 K. The temperature dependence of the magnetic entropy S was calculated by numerical integration of C_{mag}/T with respect to T (Fig. 13(b)). The results of the magnetic susceptibility measurements of $\gamma\text{-Yb}_2\text{S}_3$ indicate that the valence of the Yb ions is trivalent. The ground-state of Yb^{3+} ($4f^{13}$) is $^2F_{7/2}$ by Hund's rules. The ground-state multiplet of $J = 7/2$ is split into two doublets and one quartet by cubic symmetric crystalline electric field (CEF). The magnetic entropy related with the upturn at low temperature is close to $R \ln 2$. This suggests CEF ground state is a doublet rather than a quartet. The broad peak around 150 K in C_{mag} could be Shottky anomaly CEF level splitting. The observed similarity to the theoretical curve that the ground state doublet (0) and the excited state quartet (400 K) implies that the splitting is approximately 400 K.

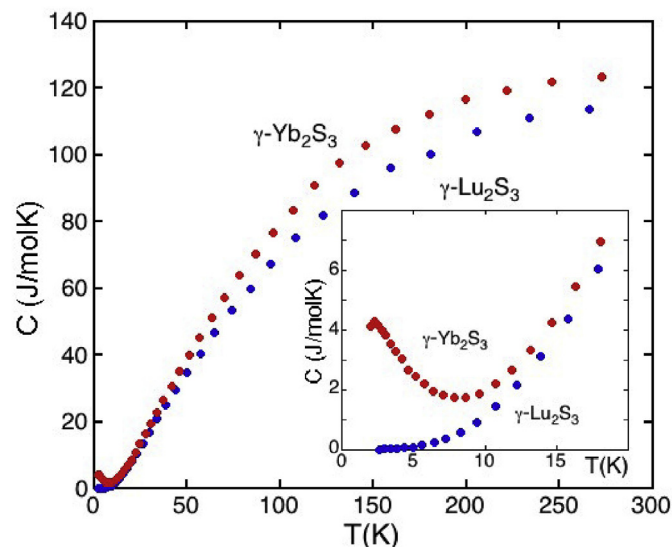


Fig. 12. Temperature dependence of the specific heat for $\gamma\text{-Yb}_2\text{S}_3$ and $\gamma\text{-Lu}_2\text{S}_3$.

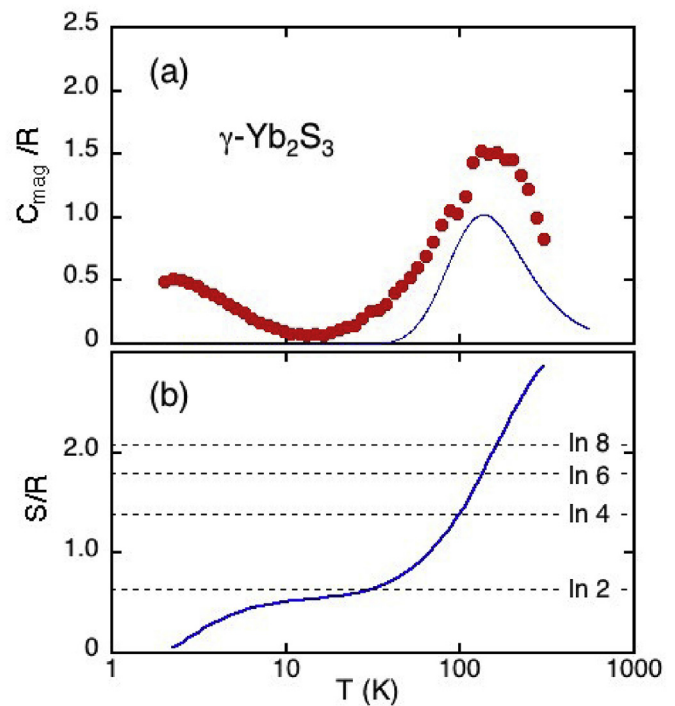


Fig. 13. (a) Temperature dependence of the magnetic specific heat for $\gamma\text{-Yb}_2\text{S}_3$. Solid line represents contribution calculated from Yb^{3+} ($4f^{13}$) $^2F_{7/2}$, 0 (doublet) and 400 K (quartet). (b) Temperature dependence of the magnetic entropy for $\gamma\text{-Yb}_2\text{S}_3$.

4. Summary

In this study, using the ζ -phase ($Fddd$) as the starting materials, the phase diagrams of Yb_2S_3 and Lu_2S_3 were investigated for the first time. Furthermore, we expanded the temperature and pressure region of the phase diagrams using elements as the starting materials. The P-T phase diagram of Lu_2S_3 is basically similar to that of Yb_2S_3 . However, the sequence of each crystal structure shifts to much higher temperature and pressure region for Lu_2S_3 . In order to obtain single phases of $\gamma\text{-Yb}_2\text{S}_3$ and $\gamma\text{-Lu}_2\text{S}_3$, appropriate temperature and pressure conditions are needed (for $\gamma\text{-Yb}_2\text{S}_3$, pressure above 2.5 GPa and temperature above 1400 °C, for $\gamma\text{-Lu}_2\text{S}_3$, pressure range between 5 and 7 GPa, above 1600 °C). Based on the P-T phase diagram, we succeeded in synthesizing single γ -phase ($I\bar{4}3d$) of the compounds under high pressure and the low-temperature transport, thermal and magnetic properties of the samples were investigated. Further research on specific heat below 2 K would be desirable to clarify the magnetic order of $\gamma\text{-Yb}_2\text{S}_3$. Thermoelectric and optical properties are currently in progress.

Acknowledgments

This work was partially supported by the Joint Usage/Research Center PRIUS, Ehime University (Proposal No. 2014A19). The synchrotron radiation experiments were performed at the BL04B1 of SPring-8 with the approval of the Japan Synchrotron Radiation Research Institute (JASRI) (Proposal No. 2013B1062) and performed under the approval of the Photon Factory Program Advisory Committee (Proposal No. 2013G124, No. 2015G031).

References

- [1] K.-J. Range, K.G. Lange, H. Drexler, Structural relations and phase transformations in the rare-earth sesquisulfide series at high pressure and temperature, *Comments Inorg. Chem.* 3 (1984) 171–188.

- [2] M. Ohta, S. Hirai, T. Mori, Y. Yajima, T. Nishimura, K. Shimakage, Effect of non-stoichiometry on thermoelectric properties of γ -Tb₂S_{3-x}, *J. Alloys Compd.* 418 (2006) 209–212.
- [3] M. Ohta, H. Yuan, S. Hirai, Y. Yajima, T. Nishimura, K. Shimakage, Thermoelectric properties of Th₃P₄-type rare-earth sulfides Ln₂S₃ (Ln = Gd, Tb) prepared by reaction of their oxides with CS₂ gas, *J. Alloys Compd.* 451 (2008) 627–631.
- [4] G. Cunningham, Y. Shen, K.L. Bray, Effect of pressure on luminescence properties of Ce³⁺:Lu₂S₃, *Phys. Rev. B* 65 (2001), 024112 (5 pages).
- [5] N.L. Eatough, A.W. Webb, H.T. Hall, High-pressure Th₃P₄-type polymorphs of rare earth sesquichalcogenides, *Inorg. Chem.* 8 (1969) 2069 (4 pages).
- [6] S.J. Kim, J.W. Anderegg, H.F. Franzen, Structural of new intermediate Lu_{2+x}S₃ phase, *J. Less Common Met.* 157 (1990) 133–138.
- [7] N. Nishiyama, Y. Wang, T. Sanehira, T. Irifune, M.L. Rivers, Development of the multi-anvil assembly 6-6 for DIA and D-DIA type high-pressure apparatuses, *High Press. Res.* 28 (2008) 307–314.
- [8] C. Sekine, H. Kato, M. Kanazawa, Y. Kawamura, K. Takeda, M. Matsuda, K. Kihou, C.-H. Lee, H. Gotou, In-situ observation of synthesizing process of Mm_xCo₄Sb₁₂ utilizing x-ray diffraction under high temperatures and high pressures, *J. Phys. Conf. Ser.* 502 (2014), 012017 (4 pages).
- [9] W. Ustumi, K. Funakoshi, Y. Katayama, M. Yamakata, T. Okada, O. Shimomura, High-pressure science with a multi-anvil apparatus at SPring-8, *J. Phys. Condens. Matter* 14 (2002) 10497–10504.
- [10] L. Li, S. Hirai, H. Yuan, Influences of Yb₂O₃ characters and sulfurization condition on preparation Yb₂S₃, *J. Alloys Compd.* 618 (2015) 742–749.
- [11] C. Sekine, T. Kawata, Y. Kawamura, T. Yagi, Thermoelectric properties of the Kondo semiconductor CeRu₄As₁₂ prepared under high pressure, *J. Korean Phys. Soc.* 63 (2013) 359–362.
- [12] C. Sekine, Y. Mori, Development of thermoelectric materials using high-pressure synthesis technique, *Jpn. J. Appl. Phys.* 56 (2017), 05FA09 (6 pages).
- [13] A.A. Eliseev, G.M. Kuzmicheva, V.V. Evdokimova, V.I. Novokshonov, Preparation of ytterbium sulfides at high pressures and temperatures, *Russ. J. Inorg. Chem.* 21 (1976) 1600–1602.
- [14] K.-J. Range, K.G. Lange, A. Gietl, Rare earth sulphide oxides Ln₂S₂O (Ln=Er, Tm, Yb): high pressure synthesis and crystal structure, *J. Less Common Met.* 158 (1990) 137–145.
- [15] A. Grzechnik, High-pressure phase transformations in Lu₂S₃, *J. Alloys Compd.* 299 (2000) 137–140.
- [16] F. Birch, Finite elastic strain of cubic crystals, *Phys. Rev.* 71 (1947) 809–824.
- [17] G.G. Gadzhiev, Sh. M. Ismailov, M.M. Khamidov, Kh. Kh. Abdullaev, V.V. Sokolov, Thermophysical properties of sulfides of lanthanum, praseodymium, gadolinium, and dysprosium, *High. Temp.* 38 (2000) 875–879.